J Nanopart Res (2014) 16:2206
DOI 10.1007/s11051-013-2206-0

RESEARCH PAPER

A comparative study of CO catalytic oxidation on Pd-anchored graphene oxide and Pd-embedded vacancy graphene

Tian-Tian Jia · Chun-Hai Lu · Yong-Fan Zhang · Wen-kai Chen

Received: 26 June 2013 / Accepted: 12 December 2013 / Published online: 12 January 2014

Abstract The catalytic oxidation of CO on Pd-anchored graphene oxide (Pd-GO) and Pd-embedded vacancy graphene (Pd-VG) is investigated by density functional theory calculations. The results validate both Pd-GO and Pd-VG show good catalytic performance for CO oxidation. Meanwhile, the more positive charge for Pd adatom and the lower reaction energy barrier make Pd-VG system slightly superior than Pd-GO system in catalytic performance. The reaction proceeds via Langmuir–Hinshelwood mechanism with a two-step route ($CO + O_2 \rightarrow OOCO \rightarrow CO_2 + O$), followed by the Eley–Rideal mechanism ($CO + O \rightarrow CO_2$). However, the synthesis of Pd-VG is more difficult in experiments compared with the readily available Pd-GO. Hence, graphene oxide may serve as the alternative substrate to deposit Pd nanoparticles.

T.-T. Jia · Y.-F. Zhang · W. Chen
Department of Chemistry, Fuzhou University, Fuzhou 350116, China

C.-H. Lu
College of Applied Nuclear Technology and Automation Engineering, Chengdu University of Technology, Chengdu 610059, China

W. Chen (✉)
Research Institute of Photocatalysis, State Key Laboratory of Photocatalysis on Energy and Environment, Fuzhou University, Fuzhou 350002, China
e-mail: wkchen@fzu.edu.cn

Keywords Pd · Graphene oxide · CO catalytic oxidation · DFT · Atmospheric pollution

Introduction

Carbon monoxide (CO), one of the contributors to atmospheric pollution, mainly comes from the inadequate combustion of fuel, vehicles as well as industrial emissions. Catalytic conversion of CO into non-toxic gas has been a continued hot topic (Turner et al. 2008; Haruta et al. 1993; Xie et al. 2009; Luo et al. 1997; Remediakis et al. 2005). However, the high reaction energy barrier often confines the oxidation of CO reaction in general temperature. In the past few decades, scientists have been constantly looking for suitable catalysts to reduce the CO reaction energy barrier and improve overall catalytic circulation rate. Of particular interest is the oxidation of CO by O_2 on transition metal surfaces (Hendriksen and Frenken 2002; Lopez and Nørskov 2002; Kim et al. 2001; Ianniello et al. 1994; Friedrich et al. 1996). Early studies from theoretical and experimental aspects demonstrated that the noble metals (Au, Pd, Pt, Rh, etc.) performed good catalytic activity and electrode material (Su et al. 1996; Remediakis et al. 2005; Zhu et al. 2007; Yates et al. 1979). CO oxidation on noble metal surface has received abundant studies. Among them, Pd, a kind of relatively cheap and abundant

resource compared to Pt and Ru, has been considered as the more anti-sintering material under the same condition (Törncrona et al. 1997). Unfortunately, such catalyst is usually restricted to be used over temperature above 100 °C for efficient catalysis (Oh and Hoflund 2007). The development of stable and active Pd-based catalysts for low-temperature CO oxidation still remains a challenge (Xie et al. 2009; Trimm and Önsan 2001).

Due to unique conductive and optical properties, graphene has been considered as the next generation of electronic material (Novoselov et al. 2004; Geim and Novoselov 2007). Moreover, the large surface area makes graphene serve as an ideal support for heterogeneous catalyst (Li et al. 2011; Zhou et al. 2010). Pd atom deposited on graphene support has attracted considerable attention partly because of the bright prospect for enhancing catalytic efficiency and reducing consumption of the catalyst. According to previous studies, bare Pd atom deposited on inert graphene is highly mobile, which mainly attributes to the large cohesive energy between Pd nanoparticles (Suarez-Martinez et al. 2009). As a direct consequence of this, the big cohesive energy will compel Pd atoms move over graphene surface and form nanoparticle clusters. These processes may lead to catalyst sintering and diminish the catalytic activity. Currently, there are two mainly popular ways to overcome this bottleneck. One is that metal-embedded vacancy graphene (VG) (one carbon atom is substituted by a metal atom), which has been fabricated experimentally with good thermal stability (Gan et al. 2008). In theory, Au (Lu et al. 2009), Cu (Song et al. 2011), Fe (Li et al. 2010), Pt (Tang et al. 2012)-embedded vacancy graphenes have been proved to have good catalytic CO performance. It is natural to think that Pd-embedded vacancy graphene will also show a similar catalytic activity. Moreover, stimulation studies point out that the contact conductance varies as Pd > Pt > Cu > Au when metal atoms deposit on underlying graphene layer (Matsuda et al. 2007). Another more common approach is to distribute Pd nanoparticles over graphene oxide (GO). The abundance of O sites on the surface play a key role in anchoring metal atoms and preventing atomic migration, which make GO serve as another candidate for supporting metal atoms. Up to now, Pd-nanosized particle deposited on GO has been theoretically studied and experimentally synthesized (Hu et al. 2010; Chen et al. 2011; Li et al. 2012b). However, a key question whether different substrates will have significantly different impacts on the catalytic performance of Pd nanoparticles is remained. To the best of our knowledge, there is still no any theoretical and experimental report on the comparative analysis of Pd nanoparticles deposited on VG and GO.

In the present paper, we performed a systematic study on catalytic oxidation CO on both Pd-embedded vacancy graphene (Pd-VG) and Pd-anchored graphene oxide (Pd-GO) by our periodic density functional calculations. Langmuir–Hinshelwood (LH) mechanism and Eley–Rideal (ER) mechanism are discussed, respectively, for this reaction. Our calculations suggest that both of the catalysts can serve as good candidates for catalytic CO oxidation. Moreover, the lower reaction energy barrier indicates Pd-VG will exhibit relatively better catalytic behavior.

Computational details

The spin-unrestricted density functional theory (DFT) calculations were performed in this work using the Dmol^3 package (Delley 2002). All results were obtained by Perdew–Wang exchange–correlation functional (PW-91) within the generalized gradient approximation (GGA; Perdew and Wang 1992). The valence electron wave functions were expanded by a double-numeric quality basis with polarization functional (DNP). 5 × 5 graphene unit cell was chosen for all of the calculations. The modulus unit cell vector was set to 20 Å in the z direction, large enough to avoid the spurious interaction with its own periodic image. Brillouin zone integration was performed with 4 × 4 × 1 k-point sampling for the geometric optimization and the search for the transition state. Monkhorst–Pack 15 × 15 × 1 k-point sampling was selected for calculation of density of state (DOS) and frontier molecular orbitals. During the geometrical optimization, all structures were relaxed until the maximum force converged to less than 2×10^{-3} Hartree/Å, the total energy was converged to within 1×10^{-5} Hartree, and the maximum displacement convergence was 5×10^{-3} Å. In order to obtain the minimum energy pathway (MEP) for catalytic oxidation of CO, linear synchronous transit (LST/QST) combined with nudged elastic band (NEB) method (Henkelman et al. 2000) was used in this work. The adsorption energy (E_{ads}) can be defined as

$$E_{ads} = E_{Pd-VG/Pd-GO} + E_{adsorbate} - E_t$$

where $E_{Pd\text{-}VG/Pd\text{-}GO}$, $E_{adsorbate}$, and E_t represent the total energies of Pd-VG or Pd-GO, the adsorbed molecule, and the total adsorption system, respectively.

Results and discussion

The supported Pd catalyst on GO and VG

Based on preliminary reported works, the deposition of Pd nanoparticles on graphene sheet was investigated in two alternative ways, labeled as Pd-GO and Pd-VG. The bind of a Pd atom on the GO was first studied. Even though various GO structural models have been proposed (Wang et al. 2009; Yan and Chou 2010; Lahaye et al. 2009; Xiang et al. 2010; Yan et al. 2009), the detailed atomic structures are still not clear (Gao et al. 2009; Jeong et al. 2008; Saxena et al. 2010; Lerf et al. 1998), due to the oxidation levels and the random distribution of oxygen-containing groups largely depend on the synthesis processes and preparation conditions. In order to obtain the energetically favorable atomic configuration of Pd-GO, the adsorption of two epoxy groups on all possible positions within a sixfold ring (four in all) are selected as the substrates, as presented in Fig. 1a–d. Only one Pd atom is anchored on the four possible GO structures. After geometry optimization, the corresponding binding energies are 2.42, 2.24, 1.26, and 1.88 eV when Pd atom deposits on the four substrates, respectively. These results show that Pd atom prefers to be anchored on the configuration containing two neighboring epoxy groups at the same side with the binding energy of 2.42 eV, due to a stable five-membered structure is formed, as shown in Fig. 2a. Two Pd–O bonds are formed to avoid the dangling bonds, and the Pd atom is strongly anchored through an O–Pd–O bridge. Similar bridge linkages are also observed when Ni and Fe atoms deposit on GO (Zhou et al. 2012; Li et al. 2012a). Hence, this most stable configuration in this work is chosen as the Pd-GO system (see Fig. 2a). The optimized structure of the Pd-GO presents the atomic distance between the Pd and its neighboring oxygen of 1.97 Å. According to Hirshfeld population analysis, the Pd adatom donates 0.42 electrons to oxygen atoms. The positively charged Pd adatom would have some activity for the oxygen reduction reaction. On the possible clustering of Pd atoms after they deposited on GO, we also computed the energy barrier for Pd diffusion. The result shows 1.55 eV diffusion barriers are big enough to hinder the dispersion of Pd atom.

A 5 × 5 lateral supercell with a single carbon atom substituted by Pd atom was selected as Pd-VG substrate (see Fig. 2c). It is found that the Pd atom strongly bonds with the neighboring three C atoms. At the same time, the Pd atom protrudes upward from the graphene sheet, due to the radius of Pd is larger than that of C atom. The calculated 1.95 Å averaged Pd–C bond length is in good agreement with the report by Suarez-Martinez et al. (2009). Hirshfeld population analysis shows that the Pd adatom donates more electrons (0.54 e) to VG. The shorter Pd–C bond length and more electrons transfer indicate much stronger covalent interaction between the Pd adatom and VG. The positively charged Pd adatom may be more advantage in catalytic reduction, which will be discussed later. The binding energy and diffusion barrier of Pd on VG are increased up to 5.63 and 4.62 eV, respectively.

Different electronic structures often result in different catalytic activity. The electronic density of states (DOS) plots of 4d, 5s and 5p orbitals of Pd atom, and the 2p, 2s orbitals of neighboring O atoms are shown in Fig. 2b. Due to the formation of Pd–O bonds, the Pd-4d, Pd-5s, and Pd-5p orbitals are partially occupied. Meanwhile, Pd-4d state splits into three sharp peaks and a widen peak below the Fermi level (E_F). The 4d peaks overlap with the neighboring O-2p state and dominate the main hybridization between Pd atom and the adjacent O atoms. In contrast to the Pd-GO system, the electronic structure of Pd-VG system undergoes significant changes as distinctly displayed in Fig. 2d. Obviously, a broadened 4d peak without splitting appears below the E_F when Pd atom is embedded into vacancy graphene. Besides, the height of 4d peak reduces associated with moving to the lower energy level explain the more electrons transferred from Pd atom to the graphene sheet (0.54 e). Hence, both the GO and VG act as electron withdrawing support. To gain more detailed insight into the electronic structure of Pd-GO and Pd-VG systems, the frontier molecular orbitals are also depicted and have been presented in Fig. 3a–d. It is clear that HOMO and LUMO dominantly locate on the Pd atom, and both of them illustrate the strong d-orbital characteristics of

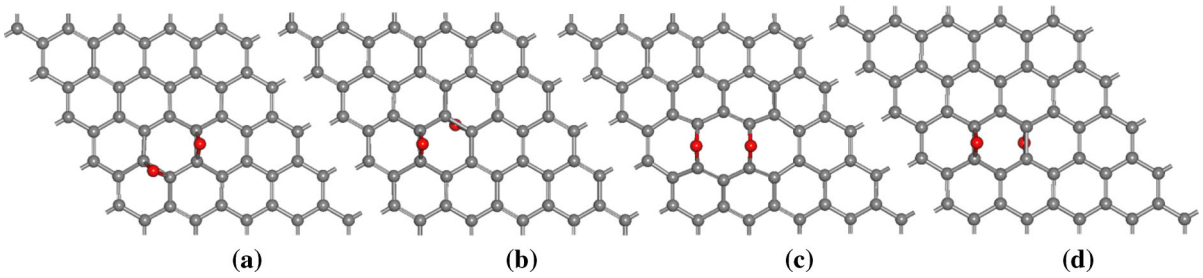

Fig. 1 Four kinds of possible graphene oxide containing two epoxy groups within a sixfold ring for anchoring Pd atom, *Gray* and *red balls* represent carbon and oxygen atoms, respectively. (Color figure online)

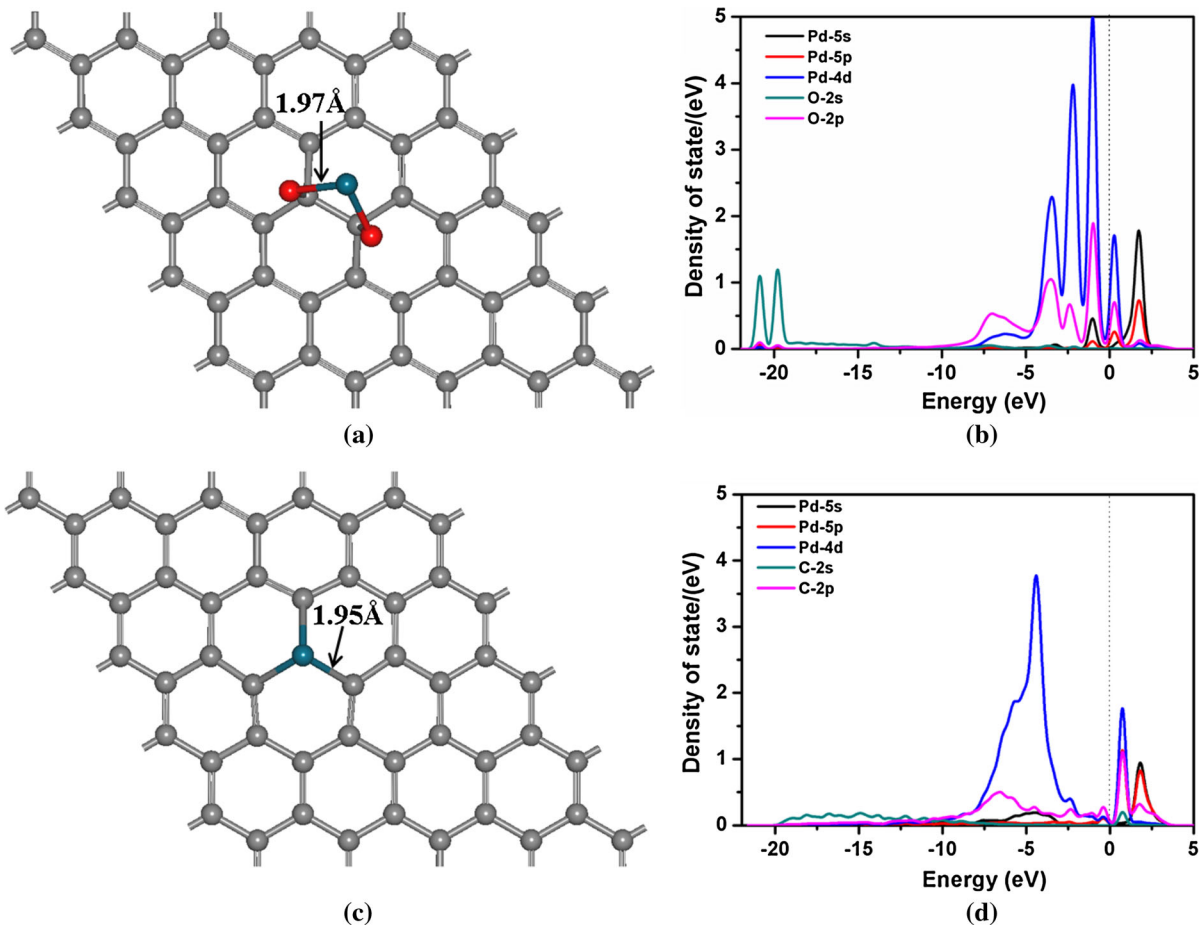

Fig. 2 The geometric and electronic structures of **a**, **b** Pd-GO, and **c**, **d** Pd-VG. The Fermi level was set to zero. *Gray*, *red*, and *blue balls* represent carbon, oxygen, and palladium atoms, respectively. (Color figure online)

the Pd atom. However, the shapes of LUMO and HOMO are drastically different in the case of Pd-VG and Pd-GO. All of these observations demonstrate that the different electronic states of Pd atom may have some influences on the catalytic property that would be discussed in the following sections.

Adsorption of CO and O_2 on Pd-VG and Pd-GO

The reaction pathways are usually determined by the adsorption ability of gas molecule on the catalyst. Herein, we first investigate the adsorption of CO on Pd-VG. All possible adsorption sites were examined in

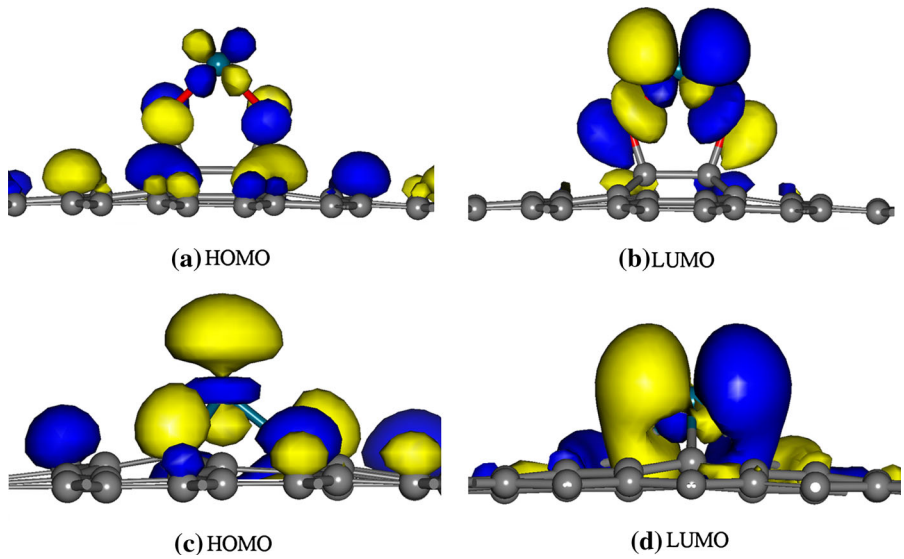

Fig. 3 Frontier molecular orbitals of the **a**, **b** Pd-GO and **c**, **d** Pd-VG, the contour value is ± 0.03 eA^{-3}. *Gray*, *red*, and *blue balls* represent carbon, oxygen and palladium atoms, respectively. (Color figure online)

order to find out the most stable adsorption configuration for each adsorbate. The maximum adsorption energy and the corresponding geometric parameters are listed in Table 1. The most stable structure with end-on configuration of CO on Pd-VG is shown in Fig. 4a with an E_{ads} of 1.07 eV. The value is in approximative with the adsorption of CO on single Pd atom (Bertin et al. 2006). Meanwhile, there are about 0.01 electrons transferring from the Pd-VG to the adsorbed CO, which occupy the CO $2\pi^*$ orbital and lead to the elongation of the C–O bond from 1.14 to 1.15 Å. The hybridization between Pd-4d and CO-$2\pi^*$ orbitals is observed near E_F from the depicted DOS in Fig. 4b. Compared with the bare Pd-VG, Pd 4d state is slightly elevated around -10.55, -7.94 and -4.21 eV below E_F, which essentially means 4d orbital of Pd atom hybridizes with CO frontier molecular orbital (FMO). The most favorable configuration of O_2 adsorption on Pd-VG is that O–O bond parallels to the graphene surface with an E_{ads} of 1.13 eV, as shown in Fig. 4c. From the energetic point of view, the O_2 adsorption configuration is slightly favorable than the configuration of CO. Meanwhile, there are about 0.40 electrons transferring from Pd-VG to O_2, which occupy the O_2-$2\pi^*$ orbital and lead to the elongation of the O–O bond from 1.22 to 1.36 Å. The elongation of the O–O bond length means that oxygen molecule can easily dissociate in reaction, which will be discussed later. Unlike the case of CO adsorption on Pd-VG, the hybridization between Pd and O atomic orbitals reduces the 4d peaks of Pd due to the electrons transfer from Pd atom to O atoms, as shown in Fig. 4d. As expected, the atomic O strongly binds with the Pd atom with adsorption energy of 4.09 eV. In addition, we also investigated various possible adsorption sites for the CO_2 molecule. The results show that there is no obvious chemical bond being observed between CO_2 and Pd atom, suggesting that CO_2 molecule is weakly physisorbed on Pd-VG and can easily desorb from graphene surface at room temperature.

Table 1 Adsorption energy (E_{ads}), adsorption height (h), bond length of adsorbate (d) and the electrons transferred from the substrate to the adsorbate (Δq) of the most stable configurations for various adsorbates on Pd-GO and Pd-VG

Adsorbate	E_{ads} (eV)	h (Å)	d (Å)	Δq (e)
Pd-GO				
CO	2.11	1.99	1.15	−0.05
O_2	1.56	2.03	1.33	−0.26
CO_2	0.61	2.26		0.08
O	3.58	1.80		−0.34
Pd-VG				
CO	1.07	2.05	1.15	−0.01
O_2	1.13	2.11	1.36	−0.40
CO_2	0.36	2.60		0.04
O	4.09	1.79		−0.43

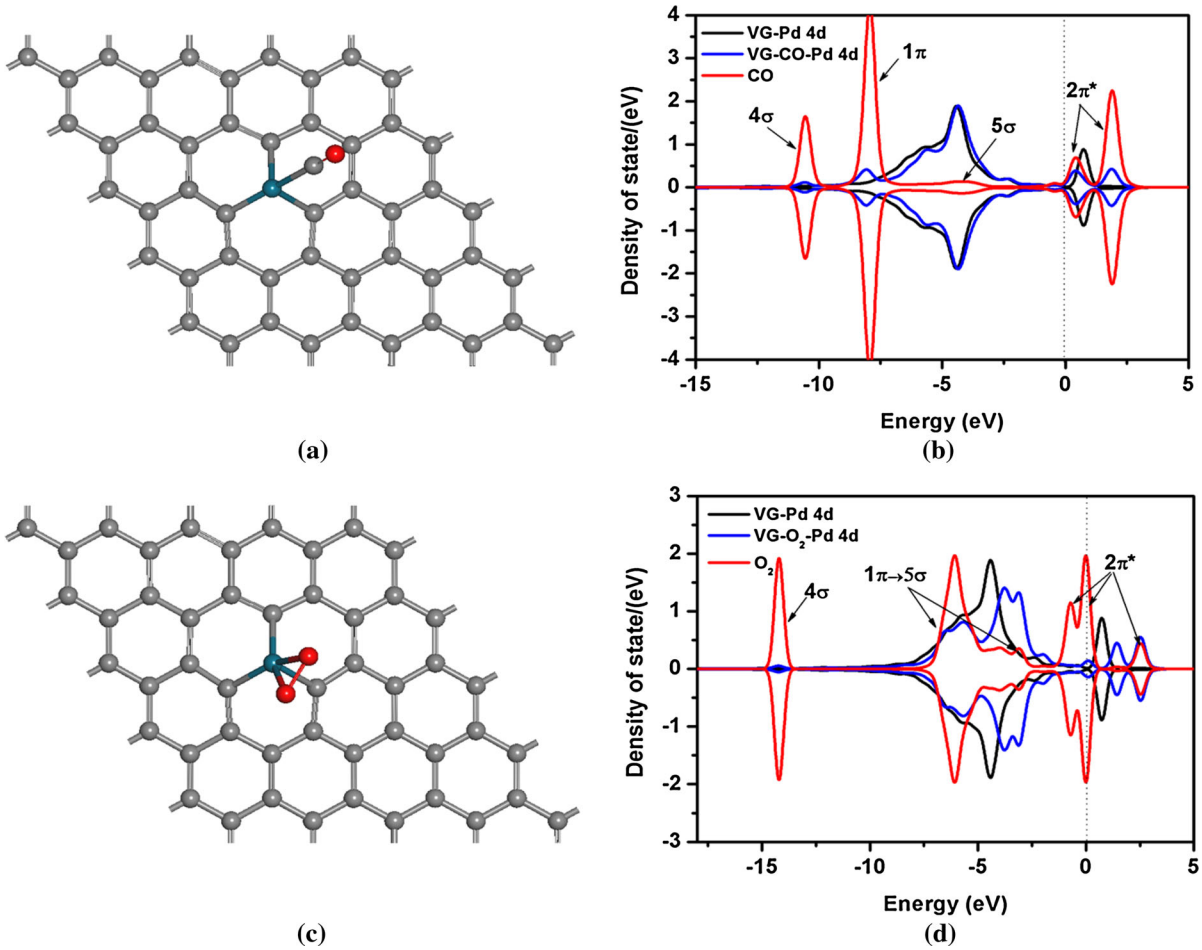

Fig. 4 Geometric and electronic structures of adsorbed system for **a**, **b** CO and **c**, **d** O_2 on Pd-VG. The Fermi level was set to zero. *Gray*, *red*, and *blue balls* represent carbon, oxygen and palladium atoms, respectively. (Color figure online)

On Pd-GO, the less positively charged Pd atom enhances the CO adsorption, compared with Pd-VG. Meanwhile, the E_{ads} of O_2 on the Pd-GO is much smaller than that of CO. Only 0.26 electrons are gained by O_2, leading to the O–O bond elongate to 1.33 Å. Additionally, the CO_2 is adsorbed by Pd atom through its O-end, and Pd–O bond is formed with an E_{ads} of 0.61 eV. Similar to Pd-VG, the atomic O is strongly bounded with the Pd atom ($E_{ads} = 3.58$ eV). In stark contrast to Pd-VG, Pd-GO may be slightly less favorable for CO oxidation.

Reaction mechanism for the CO oxidation

Eley–Rideal and Langmuir–Hinshelwood mechanisms are two well-established reaction mechanisms for CO + O_2 reaction. The ER mechanism involves the gas-phase CO molecule reacts directly with the preadsorbed O_2, where the rate-limiting step depends on the activation of O_2 molecule. For the LH mechanism, the coadsorbed O_2 and CO molecules react with each other, forming a peroxo-type (OOCO) complex as an intermediate state. In the final state, a CO_2 is released, leaving an isolated O atom adsorbed on Pd atom. The overall energy barrier is determined by the formation of OOCO intermediate state. According to previous discussion, the favorable adsorption energy of CO (2.11 eV) compared with O_2 (1.56 eV) on the Pd-GO indicates that Pd atom may be dominantly covered by CO when CO and O_2 mixture are injected as the reaction gases. Thus, the ER mechanism is unfavorable. In this case, the LH mechanism is expected to prevail for CO oxidation on Pd-GO. On Pd-VG catalyst, the much little adsorption energies difference of O_2 and CO

molecules (1.13 and 1.07 eV), indicating that both of them can be adsorbed on the Pd atom at room temperature. Besides, adsorption of the O_2 molecule is preferred rather than the CO molecule. On the other hand, the weakening of the O–O bond strength and the elongation of the O–O bond (1.36 Å) indicate O_2 molecule can be efficiently activated by Pd-VG.

The most stable coadsorption configuration of CO and O_2 on Pd-GO is studied as initial state (IS) for LH mechanism (see Fig. 5a). The similar configuration is also found on Pt-graphene catalytic stystem, in which O_2 and CO are titled to the graphene substrate (Tang et al. 2012). Meanwhile, the adsorption of CO + O_2 involves to an exothermic process with E_{ads} (CO + O_2) = 2.69 eV, being larger than E_{ads} (O_2) and E_{ads} (CO). A physisorbed CO_2 molecule and a chemisorbed atomic O bound with Pd atom are set as the final state (FS). Nudged elastic band (NEB) method was used to search the minimum energy pathway (MEP). The reaction path profile is summarized in Fig. 5a, b, and the key structural parameters are listed in Table 2. At the beginning, the O–O bond lengthe in O_2 molecule, labled as d_{O1-O2} is slightly elongated to 1.28 Å (1.24 Å in free gas phase), while the C–O bond length (d_{C-O}) is almost unchanged. In the reaction path, one of the O atoms starts to approach CO to reach the transition state (TS), meanwhile, d_{O1-O2} is elongated to 1.36 Å, and the oxygen molecule configuration is still maintained. The energy barrier between IS and TS is estimated to be 0.62 eV and is well agreement with the case of CO oxidation on GO-supported Pd_7 cluster (0.67 eV; Bertin et al. 2006). Passing over the TS, a peroxo-type OOCO complex is formed on Pd atom. After a sharp drop in energy, the whole system reaches the FS, leaving an isolated O2 atom and a physisorbed CO_2 on the GO sheet. Interestingly, this process is spontaneous without any energy barriers. A similar phenomenon is also observed on the Pt–graphene catalyst (Tang et al. 2012). The next step involves CO oxidation by the isolated O2 atom via ER mechanism. Several possible CO configurations are chosen to be attracted by the atomic O2 from different directions in the distance of 3 Å. Only 0.08 eV energies are needed to overcome the reaction barrier, and a CO_2 molecule is adsorbed on the Pd-GO surface in the FS. The slightly small E_{ads} value of CO_2 on Pd-GO (0.61 eV) indicates that CO_2 can be desorbed from Pd-GO surface easily. Compared with the commonly used Pd catalyst (Chen et al. 2007; Salo et al. 2002; Stuve et al. 1984), Pd-GO system shows the higher efficiency and activity for catalytic CO oxidation.

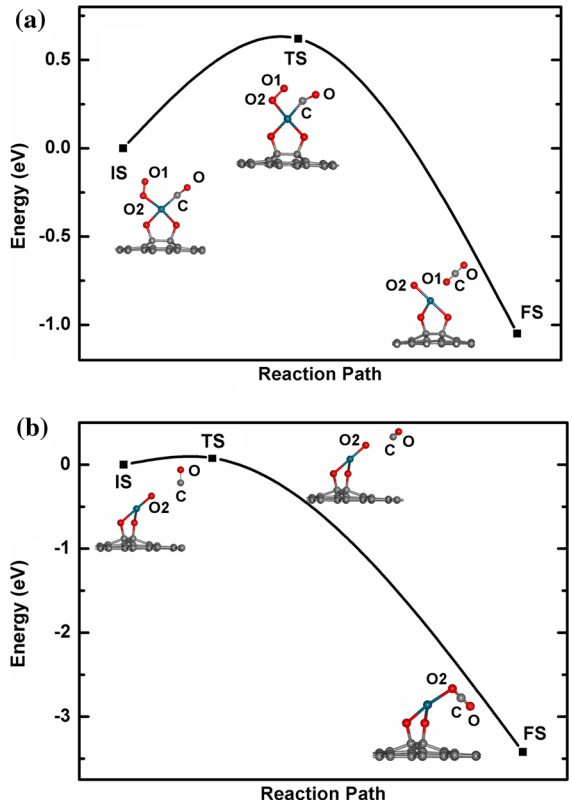

Fig. 5 **a** The LH reaction of CO + O_2 → OOCO → CO_2 + O on Pd-GO including atomic configurations at various states and corresponding reaction path. **b** The ER reaction of CO + O → CO_2 on Pd-GO including atomic configurations at various states and corresponding reaction path. *Gray*, *red*, and *blue balls* represent carbon, oxygen and palladium atoms, respectively. (Color figure online)

For Pd-VG system, both ER and LH mechanisms are studied to clarify the preferable CO catalytic oxidation pathway. The ER mechanism which involves that the physisorbed CO molecule directly reacting with the preadsorbed O_2 is firstly explored, and the atomic configurations along the reaction path are displayed in Fig. 6a. At first, CO starts to approach the activated O_2 from a distance of 3 Å, namely, initial state (IS), meanwhile the O1–O2 bond d_{O1-O2} is elongated accompanied with the approaching of CO molecule. Passing over a transition state 1 (TS1), the CO molecule inserts into the oxygen molecule and forms a carbonate-like intermediate state (MS). The

Table 2 Structural parameters for coadsorption of CO and O_2 along the MEP on the Pd-GO: (a) $CO + O_2 \rightarrow OOCO \rightarrow CO_2 + O$ and (b) $CO + O \rightarrow CO_2$. Atomic configuration at various states are displayed in Fig. 5a, b

(a)	IS	TS	FS
$d_{(C-O)}$	1.15	1.17	1.17
$d_{(C-Pd)}$	1.92	1.96	3.54
$d_{(C-O1)}$	3.04	1.78	1.17
$d_{(O1-O2)}$	1.28	1.36	2.95
$d_{(O2-Pd)}$	2.02	1.99	1.84
∠(O–C-O1)	115.74	115.42	179.65
(b)	IS	TS	FS
$d_{(C-O)}$	1.14	1.14	1.17
$d_{(C-Pd)}$	4.75	4.10	2.99
$d_{(C-O2)}$	3.00	2.55	1.19
$d_{(O2-Pd)}$	1.79	1.80	2.27
∠(O–C–O2)	112.39	100.13	176.71

The units of the bond distance d and the angle ∠ are Å and °, respectively

energy barrier along reaction pathway is estimated to be 0.69 eV, quite similar to the case of CO catalytic oxidation on Fe-GO (0.61 eV; Li et al. 2012a). The second step proceeds to the dissociation of the MS. Crossing over a relatively high energy barrier (1.12 eV), a CO_2 molecule is released, leaving an isolated O2 atom bound on Pd-VG surface (FS). However, it is found that the energy of MS is much lower than that of the FS, suggesting that ER mechanism is not thermally supported. Thus, the LH mechanism is expected to preferable for CO oxidation catalyzed by Pd-VG.

Atomic configuration at various states and potential-energy profiles are mapped in Fig. 6b for LH mechanism. The reaction starts from the coadsorption of O_2 and CO (IS) with an adsorption energy of 1.90 eV. Unlike Pd-GO, the O_2 molecule parallels to the Pd-VG surface, and both of the O atoms bind with Pd surface. The O1–O2 bond d_{O1-O2} is elongated to 1.35 Å with respect to gaseous O_2 (1.22 Å), while the CO molecule is tilted adsorbed on the Pd atom through its C-end, and the C–O bond (d_{C-O}) is almost unchanged (1.14 Å). An atomic O2 is chemisorbed on Pd-VG with a physisorbed CO_2 molecule nearby in our system is viewed as a FS. The corresponding geometric parameters at each state along the reaction path are listed in Table 3. Initially, there is no obvious interaction between the

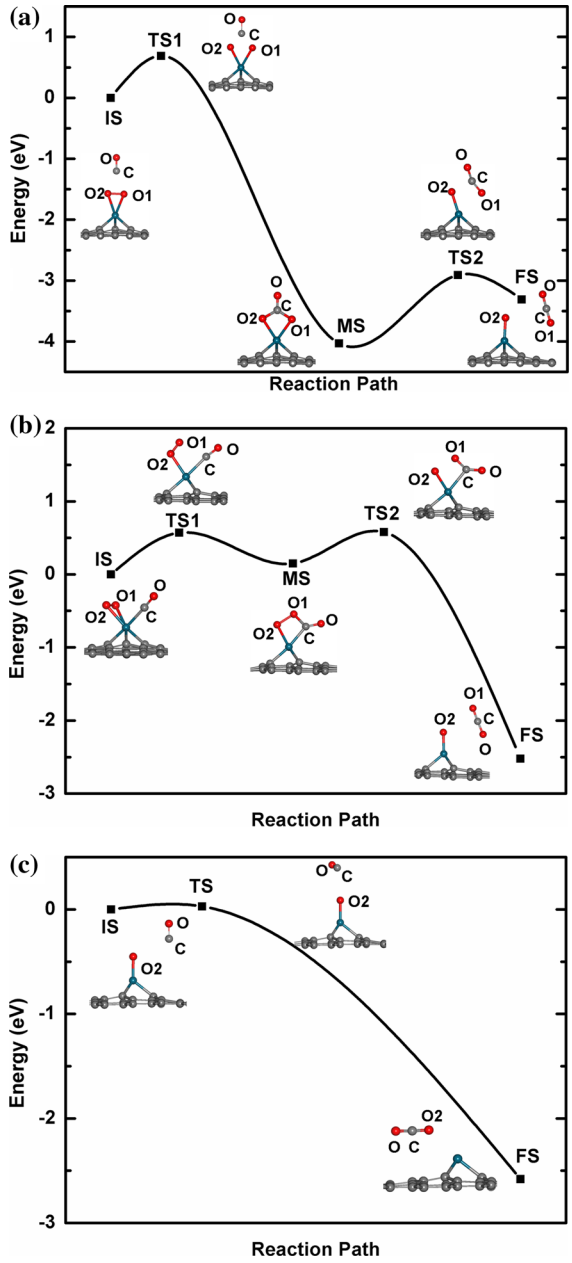

Fig. 6 **a** The ER reaction and **b** the LH reaction of $CO + O_2 \rightarrow OOCO \rightarrow CO_2 + O$ on Pd-VG including atomic configurations at various states and corresponding reaction path. **c** The ER reaction of $CO + O \rightarrow CO_2$ on Pd-VG including atomic configurations at various states and corresponding reaction path. *Gray*, *red*, and *blue balls* represent carbon, oxygen and palladium atoms, respectively. (Color figure online)

coadsorbed CO and O_2 molecules. In the reaction, the O_2 molecule turns around companying with one of the Pd-O1 bonds (d_{Pd-O1}) breaking down. At the same time, O1 atom approaches the C atom of CO and

Table 3 Structural parameters for coadsorption of CO and O_2 along the MEP on the Pd-VG: (a) $CO + O_2 \rightarrow OOCO \rightarrow CO_2 + O$ and (b) $CO + O \rightarrow CO_2$

(b)	IS	TS1	MS	TS2	FS
$d_{(C-O)}$	1.14	1.14	1.23	1.21	1.18
$d_{(C-Pd)}$	2.12	2.20	2.11	2.28	3.92
$d_{(C-O1)}$	2.88	2.44	1.42	1.25	1.17
$d_{(O1-O2)}$	1.35	1.32	1.57	1.86	3.18
$d_{(O2-Pd)}$	2.17	2.13	2.07	1.98	1.80
∠(O–C–O1)	128.69	113.78	122.08	137.59	177.82

(c)	IS	TS	FS
$d_{(C-O)}$	1.14	1.14	1.17
$d_{(C-Pd)}$	4.16	4.45	3.47
$d_{(C-O2)}$	1.79	2.66	1.18
$d_{(O2-Pd)}$	3.04	1.80	2.61
∠(O–C-O2)	115.93	97.66	178.48

Atomic configurations at various states are displayed in Fig. 6b, c. The units of the bond distance d and the angle ∠ are Å and °, respectively

reaches a transition state 1 (TS1). About 0.57 eV energy is needed to overcome the reaction energy barrier in this process. Passing over the TS1, a peroxo-type (OOCO) complex is formed, and the O1–O2 bond length d_{O1-O2} is continually elongated. Meanwhile, the OOCO complex is still maintained until d_{O1-O2} is stretched to 1.57 Å, and an intermediate state (MS) is reached. In succession, the next step involves the MS unfolds its body to release a linear CO_2 molecule. A relatively lower energy barrier (0.43 eV) is needed to overcome for transition state 2 (TS2), exhibiting a bended CO_2 molecule adsorption on Pd atom. In TS2, the distance between the O1and O2 is increased from 1.57 to 1.86 Å, and the forming C–O1 bond length (d_{C-O1}) is reduced to 1.25 Å. Passing over TS2, the final product CO_2 is released, leaving an isolated O2 atom chemisorbed on Pd-VG surface. Furthermore, we also check whether the isolated O2 atom can be easily utilized for CO oxidation. Similar to the reaction of $CO + O \rightarrow CO_2$ on Pd-GO, ER mechanism is investigated by the same method. The atomic configurations and MEP profile are displayed in Fig. 6c, and the corresponding structural parameters are also listed in Table 3. Expectedly, only 0.03 eV is needed to generate the FS along the MEP.

On the basis of the above discussions, LH mechanism is much more favorable than ER mechanism for CO and O_2 reaction on both Pd-GO and Pd-VG systems. The reaction path can be viewed as a two-step process: the first step of $CO + O_2 \rightarrow OOCO \rightarrow CO_2 + O$ is started via the LH mechanism, followed by the ER mechanism of $CO + O \rightarrow CO_2$. It is found that the catalytic oxidation CO on Pd-GO has an energy barrier of 0.62 eV for the first step, while the dissociation of OOCO complex is spontaneous without any energy barrier. In contrast to the production of CO_2 on Fe-GO (Li et al. 2012a), Pd-GO exhibits better catalytic activity. The second CO_2 is produced via ER reaction ($CO + O \rightarrow CO_2$) with much smaller energy barrier (0.08 eV). For the CO oxidation on Pd-VG, a relative lower energy barrier of 0.57 eV is needed to form a peroxo-type OOCO complex for the first step. However, 0.43 eV energies are needed to dissociate the OOCO complex and to release CO_2. Note that, the overall barrier is just determined by the highest reaction energy barrier, namely, only 0.57 eV energy barriers are needed to overcome in this step. Expectedly, 0.03 eV energies are needed to produce the second CO_2. The highest energy barrier of 0.57 eV is much lower than that has been found in the experimental value of 1.47 eV for CO oxidation on Pd (111) (Conrad et al. 1974). Consequently, Pd-VG can serve as an efficient catalyst for CO oxidation. Note that, although Pd-VG performs the better catalytic activity, the synthesis of Pd-embedded vacancy graphene is not easy in experiments compared with the readily available Pd-GO (Rodríguez-Manzo et al. 2010; Chen et al. 2011; Hu et al. 2010). The higher production cost may impede their general use in large scale production. Thus, a good trade off between production cost and catalytic performance must be considered. In this regard, GO may serve as the alternative substrate to deposit Pd nanoparticles.

Conclusions

Density functional theory calculations on the basis of first-principle method have been employed to investigate the reaction mechanism of CO oxidation by O_2. Two novel materials that consist of an isolated Pd atom deposited on single vacancy graphene as well as graphene oxide are used as catalysts. The results show that the electronic structure of the Pd atoms can be

effectively modified due to the influence of different graphene substrates, causing different effects on the catalytic activities. In the first step, the LH reaction mechanism is favorable than ER reaction mechanism on both Pd-VG and Pd-GO. Moreover, Pd-VG shows slightly higher catalytic activity for CO oxidation with a lower activation barrier of 0.57 eV (0.62 eV on the Pd-GO). The second step involves the ER mechanism with a much smaller energy barrier of 0.03 eV (0.08 eV on the Pd-GO). It is noted that even though Pd-VG performs the better catalytic activity for CO oxidation, a good trade off between production cost and catalytic performance must be considered. In this regard, the little difference of energy barrier may make GO serves as the alternative substrate to deposition of Pd nanoparticles.

Acknowledgments The Project was supported by the Foundation of State Key Laboratory of Coal Combustion of Huazhong University of Science and Technology (FSKLCC1110) and the Natural Science Foundation of Fujian Province, China (2012J01041).

References

Bertin V, Agacino E, López-Rendon R, Poulain E (2006) The CO chemisorption on some active sites of Pd clusters: a DFT study. J Mol Struc 769(1):243–248. doi:10.1016/j.theochem.2006.04.026

Chen MS, Cai Y, Yan Z, Gath KK, Axnanda S, Wayne Goodman D (2007) Highly active surfaces for CO oxidation on Rh, Pd, and Pt. Surf Sci 601(23):5326–5331. doi:10.1016/j.susc.2007.08.019

Chen XM, Wu GH, Chen JM, Chen X, Xie ZX, Wang XR (2011) Synthesis of "clean" and well-dispersive Pd nanoparticles with excellent electrocatalytic property on graphene oxide. J Am Chem Soc 133(11):3693–3695. doi:10.1021/ja110313d

Conrad H, Ertl G, Koch J, Latta E (1974) Adsorption of CO on Pd single crystal surfaces. Surf Sci 43(2):462–480. doi:10.1016/0039-6028(74)90270-2

Delley B (2002) Hardness conserving semilocal pseudopotentials. Phys Rev B 66(15):155125. doi:10.1103/PhysRevB.66.155125

Friedrich KA, Geyzers K-P, Linke U, Stimming U, Stumper J (1996) CO adsorption and oxidation on a Pt (111) electrode modified by ruthenium deposition: an IR spectroscopic study. J Electroanal Chem 402(1–2):123–128. doi:10.1016/0022-0728(95)04237

Gan Y, Sun L, Banhart F (2008) One- and two-dimensional diffusion of metal atoms in graphene. Small 4(5):587–591. doi:10.1002/smll.20070092

Gao W, Alemany LB, Ci L, Ajayan PM (2009) New insights into the structure and reduction of graphite oxide. Nat Chem 1(5):403–408. doi:10.1038/nchem.281

Geim AK, Novoselov KS (2007) The rise of graphene. Nat Mater 6(3):183–191. doi:10.1038/nmat1849

Haruta M, Tsubota S, Kobayashi T, Kageyama H, Genet MJ, Delmon B (1993) Low-temperature oxidation of CO over gold supported on TiO_2, α-Fe_2O_3, and Co_3O_4. J Catal 144(1):175–192. doi:10.1006/jcat 1993.1322

Hendriksen B, Frenken J (2002) CO oxidation on Pt (110): scanning tunneling microscopy inside a high-pressure flow reactor. Phys Rev Lett 89(4):046101. doi:10.1103/PhysRevLett.89.046101

Henkelman G, Uberuaga BP, Jónsson H (2000) A climbing image nudged elastic band method for finding saddle points and minimum energy paths. J Chem Phys 113:9901. doi:10.1063/1.1329672

Hu ZL, Aizawa M, Wang ZM, Yoshizawa N, Hatori H (2010) Synthesis and characteristics of graphene oxide-derived carbon nanosheet—Pd nanosized particle composites. Langmuir 26(9):6681–6688. doi:10.1021/la9040166

Ianniello R, Schmidt VM, Stimming U, Stumper J, Wallau A (1994) CO adsorption and oxidation on Pt and Pt–Ru alloys: dependence on substrate composition. Electrochim Acta 39(11):1863–1869. doi:10.1016/0013-4686(94)85176-X

Jeong HK, Lee YP, Lahaye RJ, Park MH, An KH, Kim IJ, Yang CW, Park CY, Ruoff RS, Lee YH (2008) Evidence of graphitic AB stacking order of graphite oxides. J Am Chem Soc 130(4):1362–1366. doi:10.1021/ja076473o

Kim M, Bertram M, Pollmann M, von Oertzen A, Mikhailov AS, Rotermund HH, Ertl G (2001) Controlling chemical turbulence by global delayed feedback: pattern formation in catalytic CO oxidation on Pt (110). Science 292(5520):1357–1360. doi:10.1126/science.1059478

Lahaye R, Jeong H, Park C, Lee Y (2009) Density functional theory study of graphite oxide for different oxidation levels. Phys Rev B 79(12):125435. doi:10.1103/PhysRevB.79.125435

Lerf A, He H, Forster M, Klinowski J (1998) Structure of graphite oxide revisited. J Phys Chem B 102(23):4477–4482. doi:10.1021/jp9731821

Li YF, Zhou Z, Yu GT, Chen W, Chen ZF (2010) CO catalytic oxidation on iron-embedded graphene: computational quest for low-cost nanocatalysts. J Phys Chem C 114(14):6250–6254. doi:10.1021/jp911535v

Li YG, Wang HL, Xie LM, Liang YY, Hong GS, Dai HJ (2011) MoS_2 nanoparticles grown on graphene: an advanced catalyst for the hydrogen evolution reaction. J Am Chem Soc 133(19):7296–7299. doi:10.1021/ja201269b

Li F, Zhao J, Chen Z (2012a) Fe-anchored graphene oxide: a low-cost and easily accessible catalyst for low-temperature CO oxidation. J Phys Chem C 116(3):2507–2514. doi:10.1021/jp209572d

Li YZ, Yu Y, Wang JG, Song J, Li Q, Liu CJ (2012b) CO oxidation over graphene supported palladium catalyst. Appl. Catal B 125:189–196. doi:10.1016/j.apcatb.2012.05.023

Lopez N, Nørskov JK (2002) Catalytic CO oxidation by a gold nanoparticle: a density functional study. J Am Chem Soc 124(38):11262–11263. doi:10.1021/ja026998a

Lu Y, Zhou M, Zhang C, Feng Y (2009) Metal-embedded graphene: a possible catalyst with high activity. J Phys Chem C 113(47):20156–20160. doi:10.1021/jp908829m

Luo MF, Zhong YJ, Yuan XX, Zheng XM (1997) TPR and TPD studies of CuO/CeO_2 catalysts for low temperature CO

oxidation. Appl Catal A 162(1):121–131. doi:10.1016/S0926-860X(97)00089-6

Matsuda Y, Deng WQ, Goddard WA (2007) Contact resistance properties between nanotubes and various metals from quantum mechanics. J Phys Chem C 111(29):11113–11116. doi:10.1021/jp072794a

Novoselov KS, Geim AK, Morozov SV, Jiang D, Zhang Y, Dubonos SV, Grigorieva IV, Firsov AA (2004) Electric field effect in atomically thin carbon films. Science 306(5696):666–669. doi:10.1126/science.1102896

Oh S, Hoflund GB (2007) Low-temperature catalytic carbon monoxide oxidation over hydrous and anhydrous palladium oxide powders. J Catal 245(1):35–44. doi:10.1016/j.jcat.2006.09.016

Perdew JP, Wang Y (1992) Accurate and simple analytic representation of the electron-gas correlation energy. Phys Rev B 45(23):13244. doi:10.1103/PhysRevB.45.13244

Remediakis IN, Lopez N, Nørskov JK (2005) CO oxidation on rutile-supported Au nanoparticles. Angew Chem 117(12):1858–1860. doi:10.1002/ange.200461699

Rodríguez-Manzo JA, Cretu O, Banhart F (2010) Trapping of metal atoms in vacancies of carbon nanotubes and graphene. ACS Nano 4(6):3422–3428. doi:10.1021/nn100356q

Salo P, Honkala K, Alatalo M, Laasonen K (2002) Catalytic oxidation of CO on Pd (111). Surf Sci 516(3):247–253. doi:10.1016/S0039-6028(02)01965-9

Saxena S, Tyson TA, Negusse E (2010) Investigation of the local structure of graphene oxide. J Phys Chem Lett 1(24):3433–3437. doi:10.1021/jz1014339

Song EH, Wen Z, Jiang Q (2011) CO catalytic oxidation on copper-embedded graphene. J Phys Chem C 115(9):3678–3683. doi:10.1021/jp108978c

Stuve EM, Madix RJ, Brundle CR (1984) CO oxidation on Pd (100): a study of the coadsorption of oxygen and carbon monoxide. Surf Sci 146(1):155–178. doi:10.1016/0039-6028(84)90235-8

Su XC, Cremer PS, Shen YR, Somorjai GA (1996) Pressure dependence (10^{-10}–700 Torr) of the vibrational spectra of adsorbed CO on Pt (111) studied by sum frequency generation. Phys Rev Lett 77(18):3858–3860. doi:10.1103/PhysRevLett.77.3858

Suarez-Martinez I, Felten A, Pireaux JJ, Bittencourt C, Ewels CP (2009) Transition metal deposition on graphene and carbon nanotubes. J Nanosci Nanotechnol 9(10):6171–6175. doi:10.1166/jnn.2009.1557

Tang Y, Yang Z, Dai X (2012) A theoretical simulation on the catalytic oxidation of CO on Pt/graphene. Phys Chem Chem Phys 14(48):16566–16572. doi:10.1039/C2CP41441D

Törncrona A, Skoglundh M, Thormählen P, Fridell E, Jobson E (1997) Low temperature catalytic activity of cobalt oxide and ceria promoted Pt and Pd: influence of pretreatment and gas composition. Appl Catal B 14(1):131–145. doi:10.1016/S0926-3373(97)00018-0

Trimm DL, Önsan ZI (2001) Onboard fuel conversion for hydrogen-fuel-cell-driven vehicles. Catal Rev 43(1–2):31–84. doi:10.1081/CR-100104386

Turner M, Golovko VB, Vaughan OP, Abdulkin P, Berenguer-Murcia A, Tikhov MS, Johnson BF, Lambert RM (2008) Selective oxidation with dioxygen by gold nanoparticle catalysts derived from 55-atom clusters. Nature 454(7207):981–983. doi:10.1038/nature07194

Wang L, Lee K, Sun Y–Y, Lucking M, Chen Z, Zhao JJ, Zhang SB (2009) Graphene oxide as an ideal substrate for hydrogen storage. ACS Nano 3(10):2995–3000. doi:10.1021/nn900667s

Xiang HJ, Wei SH, Gong XG (2010) Structural motifs in oxidized graphene: a genetic algorithm study based on density functional theory. Phys Rev B 82(3):035416. doi:10.1103/PhysRevB.82.035416

Xie XW, Li Y, Liu ZQ, Haruta M, Shen WJ (2009) Low-temperature oxidation of CO catalysed by Co_3O_4 nanorods. Nature 458(7239):746–749. doi:10.1038/nature07877

Yan JA, Chou MY (2010) Oxidation functional groups on graphene: structural and electronic properties. Phys Rev B 82(12):125403. doi:10.1103/PhysRevB.82.125403

Yan JA, Xian LD, Chou MY (2009) Structural and electronic properties of oxidized graphene. Phys Rev Lett 103(8):086802. doi:10.1103/PhysRevLett.103.086802

Yates JT Jr, Duncan TM, Vaughan RW (1979) Infrared spectroscopic study of activated surface processes: CO chemisorption on supported Rh. J Chem Phys 71(10):3908–3915. doi:10.1063/1.438159

Zhou ZH, Gao F, Goodman DW (2010) Deposition of metal clusters on single-layer graphene/Ru (0001): factors that govern cluster growth. Surf Sci 604(13):L31–L38. doi:10.1016/j.susc.2010.03.008

Zhou GM, Wang DW, Yin LC, Li N, Li F, Cheng HM (2012) Oxygen bridges between NiO nanosheets and graphene for improvement of lithium storage. ACS Nano 6(4):3214–3223. doi:10.1021/nn300098m

Zhu HQ, Qin ZF, Shan WJ, Shen WJ, Wang JG (2007) CO oxidation at low temperature over Pd supported on CeO_2–TiO_2 composite oxide. Catal Today 126(3–4):382–386. doi:10.1016/j.cattod.2007.06.012